

# A Comparison of Approximate Models for Radiation in Gas Turbines

M. Frank, M. Seaid, J. Janicka, A. Klar,  
R. Pinnau and G. Thömmes

*Fachbereich Mathematik  
Technische Universität Darmstadt  
D-64289 Darmstadt, Germany*  
and  
*Fachbereich Maschinenbau  
Technische Universität Darmstadt  
D-64289 Darmstadt, Germany*

## Abstract

Approximate equations for radiative heat transfer equations coupled to an equation for the temperature are stated and a comparative numerical study of the different approximations is given. The approximation methods considered here range from moment methods to simplified  $P_N$ -approximations. Numerical experiments and comparisons in different space dimensions and for various physical situations are presented.

**Key words.** Radiative Transfer,  $SP_N$ -Approximations, Moment Methods, Frequency averages, Discontinuous coefficients

**AMS(MOS) subject classification.**

## 1 Introduction

During the last years the interest in numerically tractable approximations to the radiative heat transfer equations drastically increased, for example because of the fact that simulation tools for modern gas turbine combustion chambers need to predict accurately the load of the walls due to thermal radiation.

In this paper we consider the radiative transfer equations stated on a bounded domain  $\mathcal{D} \subset \mathbb{R}^3$  in the form

$$\varepsilon^2 \partial_t T + \varepsilon^2 u \cdot \nabla T = \varepsilon^2 \nabla \cdot (k_0 \nabla T) + \int_{\nu_0}^{\infty} \int_{S^2} \kappa(I - B) d\Omega d\nu \quad (1.1a)$$

$$\forall \nu > \nu_0, \Omega \in S^2: \quad \varepsilon \Omega \cdot \nabla I + (\sigma + \kappa)I = \frac{\sigma}{4\pi} \int_{S^2} I d\Omega + \kappa B \quad (1.1b)$$

supplemented with boundary data

$$\varepsilon k n \cdot \nabla T = h(T_b - T) + \alpha \pi \int_0^{\nu_0} B(T_b, \nu) - B(T, \nu) d\nu \quad (1.1c)$$

$$\text{for } n \cdot \Omega < 0 : \quad I(\Omega) = \rho I(\Omega') + (1 - \rho) B(T_b(x)) \quad (1.1d)$$

In these equations,  $I(x, \Omega, \nu, t)$  denotes the specific radiation intensity for frequency  $\nu$  at point  $x \in \mathcal{D}$  travelling in direction  $\Omega \in S^2$  at time  $t \geq 0$ .  $B$  denotes Planck's function

$$B(\nu, T) = \frac{2h_P \nu^3}{c^2} \left( e^{\frac{h_P \nu}{k_B T}} - 1 \right)^{-1}$$

for black body radiation, which involves Planck's constant  $h_P$ , Boltzmann's constant  $k_B$  and the speed of light in vacuum  $c$ .  $T(x, t)$  denotes the material temperature and  $T_b$  is the exterior temperature on the boundary.  $\nu_0$  denotes the boundary of the opaque part of the spectrum. The equations contain the absorption and scattering parameters  $\kappa(\nu, T)$  and  $\sigma(\nu, T)$ .  $k_0$  is the heat conduction coefficient. The outside radiation is assumed to be known for the ingoing directions (i.e.  $n \cdot \Omega < 0$ ) on the boundary, where we denote the outward normal on  $\partial\mathcal{D}$  by  $n$ . The reflected angle is  $\Omega' = \Omega - 2(n \cdot \Omega)n$ .  $\rho = \rho(\Omega)$  denotes the part of the radiation which is reflected. Finally,  $\varepsilon$  denotes a dimensionless parameter describing the distance from an optically thick medium.

$$\varepsilon = \frac{1}{x_{ref} \kappa_{ref}},$$

where  $x_{ref}$  and  $\kappa_{ref}$  are reference length scale and reference absorption rate respectively.

Hierarchies of models approximating (1.1) have been derived by various authors, [14, 9, 11, 10, 7] and many others. They range from moment methods closed by entropy principles to diffusive methods like the  $SP_N$ -equations. Clearly, these models will differ in their accuracy and numerical complexity. They are usually faster than direct solution methods for (1.1), but less accurate.

## 2 Approximate equations

In this section we briefly describe different approximate models for the RHT equations.

### 2.1 Diffusive Approximations

The following approximations are obtained by an asymptotic procedure, see [11].

### 2.1.1 $P_1$ -Approximation

The first approximation yields a well known model approximating the transport equation (1.1) to  $\mathcal{O}(\varepsilon^2)$ . The classical  $P_1$  equation reads

$$\partial_t T + u \cdot \nabla T = \nabla \cdot (k_0 \nabla T) + \int_{\nu_0}^{\infty} \nabla \cdot \left( \frac{1}{3(\sigma + \kappa)} \nabla \Phi \right) d\nu, \quad (2.1a)$$

$$\forall \nu \geq \nu_0 : \quad -\varepsilon^2 \nabla \cdot \left( \frac{1}{3(\sigma + \kappa)} \nabla \Phi \right) + \kappa \Phi = \kappa(4\pi B), \quad (2.1b)$$

where  $\Phi \sim \int_{S^2} I d\Omega$  is the total incident radiation. System (2.1) is supplemented with Robin-type boundary data:

$$\forall \nu \geq \nu_0 : \quad \Phi(x) + \left( \frac{1 + 3r_2}{1 - 2r_1} \frac{2\varepsilon}{3(\kappa + \sigma)} \right) n \cdot \nabla \Phi(x) = 4\pi B_b(x), \quad (2.2)$$

where  $B_b(x) = B(\nu, T_b(x))$ . The boundary condition for the temperature is the same as before.  $r_i$  are values depending on the reflectivity  $\rho$ , see [11].

### 2.1.2 $SP_2$ -Approximation

The second approximation to  $\mathcal{O}(\varepsilon^4)$  is

$$\frac{\partial T}{\partial t} + u \cdot \nabla T = \nabla \cdot k_0 \nabla T + \int_{\nu_0}^{\infty} \nabla \cdot \frac{1}{3(\sigma + \kappa)} \nabla \xi \, d\nu, \quad (2.3a)$$

$$\forall \nu \geq \nu_0 : \quad -\varepsilon^2 \nabla \cdot \frac{3}{5(\sigma + \kappa)} \nabla \xi + \kappa \xi = \kappa(4\pi B), \quad (2.3b)$$

where

$$\xi = \Phi + \frac{4}{5}(\Phi - 4\pi B). \quad (2.4)$$

The boundary conditions are

$$\begin{aligned} \forall \nu \geq \nu_0 : \quad \xi(x) + \left( \frac{1 + 3r_2}{1 - 4r_3} \frac{4\varepsilon}{5(\kappa + \sigma)} \right) n \cdot \nabla \xi(x) \\ = 4\pi B(x) + \left( \frac{1 - 2r_1}{1 - 4r_3} \frac{6}{5} \right) [4\pi B_b(x) - 4\pi B(x)]. \end{aligned} \quad (2.5)$$

### 2.1.3 $SP_3$ -Approximation

The third approximation is the  $SP_3$  equation:

$$\partial_t T + u \cdot \nabla T = \nabla \cdot (k_0 \nabla T) + \int_{\nu_0}^{\infty} \nabla \cdot \left( \frac{1}{(\sigma + \kappa)} \nabla (a_1 \Psi_1 + a_2 \Psi_2) \right) d\nu, \quad (2.6a)$$

$$\forall \nu \geq \nu_0: \quad -\varepsilon^2 \nabla \cdot \left( \frac{\mu_1^2}{(\sigma + \kappa)} \nabla \Psi_1 \right) + \kappa \Psi_1 = \kappa (4\pi B), \quad (2.6b)$$

$$\forall \nu \geq \nu_0: \quad -\varepsilon^2 \nabla \cdot \left( \frac{\mu_2^2}{(\sigma + \kappa)} \nabla \Psi_2 \right) + \kappa \Psi_2 = \kappa (4\pi B). \quad (2.6c)$$

$\Phi$  is found as linear combination of  $\Psi_1$  and  $\Psi_2$ . System (2.6) is supplemented with Robin-type boundary conditions.

$$\alpha_1 \psi_1(x) + \frac{\varepsilon}{\kappa} n \cdot \nabla \psi_1(x) = -\beta_2 \psi_2(x) + \eta_1 B_b, \quad (2.7a)$$

$$\alpha_2 \psi_2(x) + \frac{\varepsilon}{\kappa} n \cdot \nabla \psi_2(x) = -\beta_1 \psi_1(x) + \eta_2 B_b. \quad (2.7b)$$

$\mu_i, a_i, \alpha_i, \beta_i, \eta_i$  are appropriate constants, see again [11]. These equations approximate the full RHT equations with order  $\mathcal{O}(\varepsilon^6)$ . For details see [9, 11]. We note that – based on the  $SP_N$  equations – one can derive frequency averaged equations. We refer to [10] for an example.

## 2.2 Entropy-Moment Approximations

These approximations are based on moment methods where the closure relation is obtained by entropy maximization.

### 2.2.1 Full Space Entropy-Moment (EM) Approximation

The Levermore entropy approach [14, 5] for radiation yields the following system for the frequency independent case  $\kappa = \text{constant}$  and  $\nu_0 = 0$ :

$$\varepsilon^2 \partial_t T + \varepsilon^2 u \cdot \nabla T = \varepsilon^2 \nabla \cdot (k_0 \nabla T) + \kappa (\Phi - 4\pi B(T)) \quad (2.8a)$$

$$\varepsilon \nabla \cdot F + \kappa \Phi = 4\pi B(T), \quad (2.8b)$$

$$\varepsilon \nabla \cdot (D(f)\Phi) + (\kappa + \sigma)F = 0. \quad (2.8c)$$

Here  $B(T)$  denotes the frequency averaged Planck function  $B(T) = \int_0^\infty B(T, \nu) d\nu = aT^4$ . The relative flux is given by  $f = F/\Phi$  and the Eddington factor is

$$D(f) = D = \frac{1 - \chi}{2} I + \frac{3\chi - 1}{2} n \otimes n, \quad n = \frac{f}{\|f\|}, \quad \chi = \frac{3 + 4\|f\|^2}{5 + 2\sqrt{4 - 3\|f\|^2}}.$$

Here,  $\Phi$  approximates the frequency averaged incident radiation  $\int_0^\infty \int_{S^2} I d\Omega d\nu$  and  $F$  is an approximation for  $\int_0^\infty \int_{S^2} \Omega I d\Omega d\nu$ . A model including frequency dependence can be found in [17]. Related models can be found in [16, 12, 2, 15, 1]. A more general approach is described in the next subsection.

### 2.2.2 Partial Space Entropy-Moment (PSEM) Approximation

For a function  $g = g(\nu, \Omega)$ , where  $\nu$  denotes frequency and  $\Omega$  denotes direction, we define

$$\langle g \rangle_A = \int_A \int_{\nu_0}^\infty g(\nu, \Omega) d\nu d\Omega.$$

Here,  $A$  denotes the set of the angular integration. For example for a half space moment model we have  $A \in \{\mathcal{S}_+^2, \mathcal{S}_-^2\}$ . Here,  $\mathcal{S}_+^2 = \{\Omega \in \mathcal{S}^2 : \Omega_x > 0\}$  is the positive half sphere and  $\mathcal{S}_-^2$  is defined analogously. We define the corresponding moments by

$$\begin{aligned}\Phi_A &= \langle \hat{I} \rangle_A \\ F_A &= \langle \Omega \hat{I} \rangle_A \\ P_A &= \langle (\Omega \otimes \Omega) \hat{I} \rangle_A.\end{aligned}$$

where  $\hat{I} = \hat{I}(\Phi_A, F_A)$  is an approximation of  $I$  found by entropy minimization. Let  $\mathcal{A}$  be a partition of the unit sphere  $\mathcal{S}^2$ . Then the moment system reads for the case of constant  $\kappa$ :

$$\begin{aligned}\varepsilon^2 \partial_t T + \varepsilon^2 u \cdot \nabla T &= \varepsilon^2 \nabla \cdot (k_0 \nabla T) + \kappa \left( \sum_{A' \in \mathcal{A}} \Phi_{A'} - \langle B(T) \rangle_{S^2} \right) \\ \varepsilon \nabla F_A + (\kappa + \sigma) \Phi_A &= \frac{\sigma}{4\pi} \langle 1 \rangle_A \sum_{A' \in \mathcal{A}} \Phi_{A'} + \kappa \langle B(T) \rangle_A \\ \varepsilon \nabla P_A + (\kappa + \sigma) F_A &= \frac{\sigma}{4\pi} \langle \Omega \rangle_A \sum_{A' \in \mathcal{A}} \Phi_{A'} + \kappa \langle \Omega B(T) \rangle_A\end{aligned}$$

for all  $A \in \mathcal{A}$ . Note, that the above is a hyperbolic system with relaxation terms as before. For a derivation in the one-dimensional case we refer to [7]. Further investigations can be found in [6, 8]. Different approaches to partial space methods can be found for example in [4]. In the computations below we use a quarter space method in 2D, dividing the angular space into 4 quadrants. Models including frequency dependence can be developed along the same lines as in the full moment case.

## 3 Numerical Comparisons for fixed temperature

### 3.1 One-dimensional situation

We specify a test configuration to compare the different models. First, we consider a *fixed* temperature profile in 1D, where the temperature increases linearly from 1000 K to 1800 K. The 1-band case is assumed with  $\sigma$  and  $\kappa$  constant. Thus, we consider in  $\mathcal{D} = [0, 1]$  the following equations:

$$\mu \frac{\partial I}{\partial x} + (\sigma + \kappa)I = \frac{\sigma}{2} \int_{-1}^1 I(x, \mu') d\mu' + \kappa B(T(x)),$$

where

$$B(T) = aT^4, T(x) = 1000 + 800x, T_b(\hat{x}) = T(\hat{x}), \rho = 0.$$

We compare in Figure 5.1-5.2 the different approximate equations for the cases  $\sigma = 1, \kappa = 1$  and  $\sigma = 0.1, \kappa = 0.01$  with the transport solution, i.e. the solution of the RHT equations. In the case considered here, especially the half moment method gives very accurate results.

A comparison of the CPU times for the solution of the full radiative transfer equation and for the solution of the approximate equations depends on the method used for the elliptic equations and on the number of angular discretizations for the full radiation problem. To solve the radiative transfer equations we have used a multi level method, compare [3]. For the solution of the diffusive equations we use a standard method. A kinetic scheme combined with a Newton iteration is used for the half space moment method. Roughly the solution of the  $SP_3$  equations takes about twice as much time as the solution of the  $P_1$  equations. The solution of the half space moment model takes about 10 times as much time and the solution of the full transport problem is between 2 and 3 orders of magnitude slower as the  $P_1$  solution.

### 3.2 Two-dimensional situations

#### 3.2.1 Constant coefficients

In the second numerical test we fix the temperature profile in the 2D unit square. We consider  $\mathcal{D} = [0, 1] \times [0, 1]$  and the equations

$$\mu \frac{\partial I}{\partial x} + \eta \frac{\partial I}{\partial y} + (\sigma + \kappa)I = \frac{\sigma}{4\pi} \int_0^\pi \int_0^{2\pi} I(x, y, \mu', \eta') \sin\eta' d\mu' d\eta' + \kappa B(T(x, y)),$$

where  $B(T) = aT^4, T(x, y) = 1000 + 400(x + y), T_b(\hat{x}, \hat{y}) = T(\hat{x}, \hat{y}), \rho = 0.$

The comparison of the direct solution with the results of the different approximate models for the case  $\sigma = 1$ ,  $\kappa = 1$  can be found in Figure 5.3. The case  $\sigma = 0.1$ ,  $\kappa = 0.01$  along the diagonal  $x = y$  and along  $y = 0.5$  is shown in Figure 5.4 and Figure 5.5, respectively.

For these computations we have used for the partial space moment approximation a quarter space method and again a kinetic scheme combined with a Newton iteration to solve the resulting nonlinear system of equations. The diffusive equations are solved using standard methods.

### 3.2.2 Discontinuous coefficients

The second two-dimensional testcase is a situation with spatially dependent discontinuous absorption coefficients  $\kappa$ . We consider a problem with  $\mathcal{D} = [0, 1] \times [0, 10]$ ,  $\mathcal{D}_0 = [0.45, 0.55] \times [4.5, 5.5]$ .  $B(T) = aT^4$  with  $T(x, y) = 1000K$  in  $\mathcal{D}_0$  and  $T(x, y) = 1800K$  in  $\mathcal{D} \setminus \mathcal{D}_0$ .  $T_b(\hat{x}, \hat{y}) = T(\hat{x}, \hat{y})$ ,  $\rho = 0$ .  $\kappa = \kappa_0$  in  $\mathcal{D}_0$  and  $\kappa = \kappa_1$  in  $\mathcal{D} \setminus \mathcal{D}_0$ .

Again the solutions of the different approximate equations are compared with the direct solution of the RHT equations. We choose  $\sigma = 1$  and consider the cases  $\kappa_0 = 3$ ,  $\kappa_1 = 1$  and  $\kappa_0 = 1$ ,  $\kappa_1 = 0.1$ , see Figure 5.6 and 5.7.

## 4 Numerical Comparisons for the full heat transfer equations

In this section we consider the radiative transfer equations as above. However, the temperature is here not fixed, but determined by the heat transfer equation described in the beginning.

### 4.1 One-dimensional situation

As before we consider as a first step a 1D situation,  $\mathcal{D} = [0, 1]$ . The equations are

$$\varepsilon^2 \partial_t T + \varepsilon^2 u \partial_x T = \varepsilon^2 k_0 \partial_{xx} T + 2\pi \int_0^\infty \int_{-1}^1 \kappa (I - B) d\mu dv$$

$$\varepsilon \mu \partial_x I + (\sigma + \kappa) I = \frac{\sigma}{2} \int_{-1}^1 I(x, \mu') d\mu' + \kappa B(T(x)).$$

$$B(T) = aT^4.$$

We consider  $\sigma = 0$ ,  $u = 0$ ,  $k_0 = 1$  and  $\varepsilon = 1$ .  $\kappa$  is chosen equal to 1 and 0.1, respectively. Here we choose Dirichlet boundary conditions:  $I(\mu) = B(T_b)$ ,  $\mu > 0$

and  $T = T_b$  with  $T_b = 1000K$  at the left boundary  $x = 0$ .  $I(\mu) = B(T_b)$ ,  $\mu < 0$  and  $T = T_b$  with  $T_b = 1800K$  on the right boundary  $x = 1$ .

A comparison of the solutions of the different approximate equations with the RHT equations can be found in Figure 5.8 - Figure 5.9 for the cases  $\kappa = 1$  and  $\kappa = 0.1$ .

A comparison of the CPU times for the solution of the full radiative transfer equation and for the solution of the approximate equations depends on the method used for the elliptic equations and on the number of angular discretizations for the full radiation problem and gives results as in the previous section.

## 4.2 Two-dimensional situations

In the second numerical test the 2D unit square  $\mathcal{D} = [0, 1] \times [0, 1]$  is considered. The equations are

$$\varepsilon^2 \partial_t T + \varepsilon^2 u \cdot \nabla T = \varepsilon^2 \nabla \cdot (k_0 \nabla T) + \left( \int_{\nu_0}^{\infty} \int_0^{\pi} \int_0^{2\pi} I(x, y, \mu', \eta') \sin \eta' d\mu' d\eta' - 4\pi B \right) d\nu$$

$$\mu \frac{\partial I}{\partial x} + \eta \frac{\partial I}{\partial y} + (\sigma + \kappa) I = \frac{\sigma}{4\pi} \int_0^{\pi} \int_0^{2\pi} I(x, y, \mu', \eta') \sin \eta' d\mu' d\eta' + \kappa B(T(x, y)).$$

Boundary conditions are Dirichlet as before. The boundary temperature  $T_b$  is chosen as a linearly increasing function from 1000 K to 1400 K on the boundaries  $x = 0$  and  $y = 0$  of the square and from 1400 K to 1800 K for the boundaries  $x = 1$  and  $y = 1$ .

The results along  $y = 0.5$  for the different approximate models can be found in Figure 5.10-5.11. We consider again an optically thicker and an optically thinner case:  $\kappa = 1$  and  $\kappa = 0.1$ .  $\sigma$  is chosen equal to 0 for both computations. The other parameters are chosen as in the 1D case.

## 4.3 Coupling with Navier Stokes

Finally, we also consider the full moment model. In the last test we couple this system to the Navier–Stokes equation and simulated a flame–like flow in 3d. The computed temperature can be found in Figure 5.12. The solution is compared with simulations relying on the  $P_1$ –equations (2.1). While there is no visible difference in the computed temperatures, we depict in Figure 5.13 the norm of the relative flux  $|f|$ . Note, that the  $P_1$  solution gives physically unreasonable results, i.e.  $|f| > 1$ . This is well known, see for example [13] and true for all diffusive approximations. In contrast the moment method gives a physically reasonable result. The bound  $|f| < 1$  is fulfilled for all moment methods constructed here.

## 5 Conclusions

All approximate models give reasonable results in situation which are sufficiently diffusive. Partial space moment models give accurate approximations even in optically thinner regimes. The numerical effort for all approximations is in general smaller than the time needed for the solution of the full RHT even if a fast iterative method is used for the later equations. A comparison and combination of these approximate methods with efficient multigrid methods for the full radiative heat transfer equations is currently under investigation.

## Acknowledgements

The authors acknowledge support from the German Research Foundation (DFG), SFB568.

## References

- [1] Brunner T. A. and J.P. Holloway. One-dimensional Riemann solvers and the maximum entropy closure. *J. Quant. Spect. Rad. Transf.*, 69:543–566, 2001.
- [2] A.M. Anile, S. Pennisi, and M. Sammartino. A thermodynamical approach to Eddington factors. *J. Math. Phys.*, 32:544–550, 1991.
- [3] C.T. Banoczi, J.M. and Kelley. A fast multilevel algorithm for the solution of nonlinear systems of conductive-radiative heat transfer equations. *SIAM J. Sci. Comput.* 19, 19:266–279, 1998.
- [4] P.J. Clause and M. Mareschal. Heat transfer in a gas between parallel plates: Moment methods and molecular dynamics. *Physical Review A*, 38:4241–4252, 1988.
- [5] B. Dubroca and J.L. Feugeas. Moment model hierachy for radiative transfer equations. *preprint*.
- [6] B. Dubroca, M. Frank, A. Klar, and G. Thömmes. Half space moment approximation to the radiative heat transfer equations. *to appear in ZAMM*, 2003.
- [7] B. Dubroca and A. Klar. Half moment closure for radiative transfer equations. *J. Comp. Phys.*, 180:1–13, 2002.
- [8] M. Frank and R. Pinnau. Analysis of a half moment model for radiative heat transfer equations. *in preparation*.

- [9] E.M. Gelbard. Simplified spherical harmonics equations and their use in shielding problems. *WAPD-T-1182, Bettis Atomic Power Laboratory*, 1961.
- [10] E. W. Larsen, G. Thömmes, and A. Klar. New frequency–averaged approximations to the equations of radiative heat transfer. *preprint*, 2002.
- [11] E.W. Larsen, G. Thömmes, A. Klar, M. Seaid, and T. Götz. Simplified  $p_n$  approximations to the equations of radiative heat transfer in glass. *J. Comp. Phys.*, 183:652–675, 2002.
- [12] C.D. Levermore. Relating Eddington factors to flux limiters. *J. Quant. Spectroscop. Radiat. Transfer*, 31:149–160, 1984.
- [13] C.D. Levermore and G.C. Pomraning. A flux limited diffusion theory. *Astrophysics Journal*, 248:321, 1981.
- [14] D. Levermore. Moment closure hierarchies for kinetic theories. *J. Stat. Phys.*, 83, 1996.
- [15] I. Müller and T. Ruggeri. *Rational Extended Thermodynamics*. Springer, New York, 1998.
- [16] H. Struchtrup. On the number of moments in radiative transfer problems. *Annals of Physics*, 266:1–26, 1998.
- [17] R. Turpault. Construction of a multigroup  $M_1$  model for the radiative transfer equation. *C.R. Acad. Sci. Paris*, 334, Série I:331–336, 2002.

## List of Figures

5.1 Incident radiation of the different models for a fixed temperature profile in 1D and $\sigma = 1, \kappa = 1$ . . . . .	11
5.2 Incident radiation of the different models for a fixed temperature profile in 1D and $\sigma = 0.1, \kappa = 0.01$ . . . . .	12
5.3 Incident radiation of the different models for a fixed temperature profile in 2D for $\sigma = 1, \kappa = 1$ . Plot along the diagonal $x = y$ . . . . .	12
5.4 Incident radiation of the different models for a fixed temperature profile in 2D for $\sigma = 0.1, \kappa = 0.01$ . Plot along the diagonal $x = y$ . . . . .	13
5.5 Incident radiation of the different models for a fixed temperature profile in 2D for $\sigma = 0.1, \kappa = 0.01$ . Plot along $y = 0.5$ . . . . .	13
5.6 Incident radiation of the different models for discontinuous coefficients $\kappa_0 = 3, \kappa_1 = 1$ . Plot along $x = 0.5$ . . . . .	14

5.7	Incident radiation of the different models for discontinuous coefficients and $\kappa_0 = 1, \kappa_1 = 0.1$ . Plot along $y = 5$ . . . . .	14
5.8	Incident radiation of the different models for the coupled equations in 1D with $\kappa = 1$ . . . . .	15
5.9	Incident radiation of the different models for the coupled equations in 1D with $\kappa = 0.1$ . . . . .	15
5.10	Incident radiation of the different models for the coupled equations in 2D for $\kappa = 1$ . Plot along $y = 0.5$ . . . . .	16
5.11	Incident radiation of the different models for the coupled equations in 2D for $\kappa = 0.1$ . Plot along $y = 0.5$ . . . . .	16
5.12	Temperature distribution for a flame-like flow . . . . .	17
5.13	Norm of the relative flux . . . . .	17

## Figures

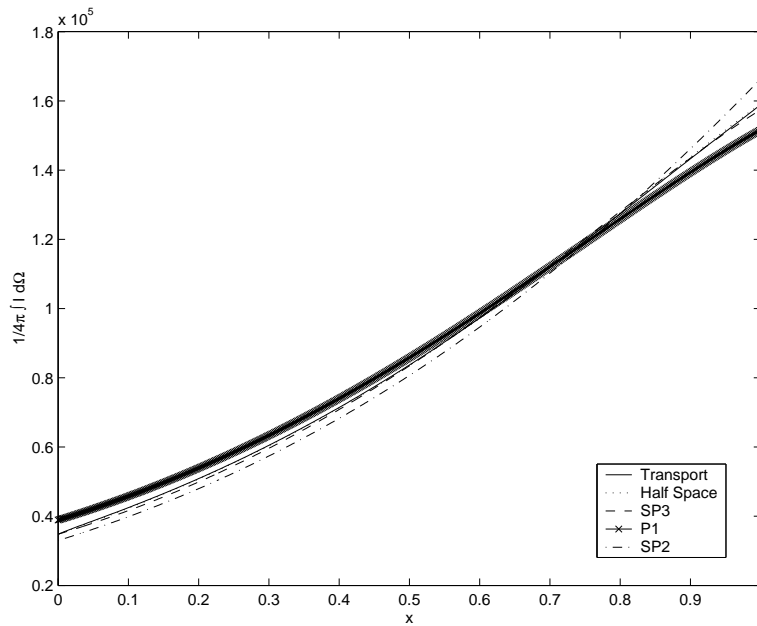


Figure 5.1: Incident radiation of the different models for a fixed temperature profile in 1D and  $\sigma = 1, \kappa = 1$ .

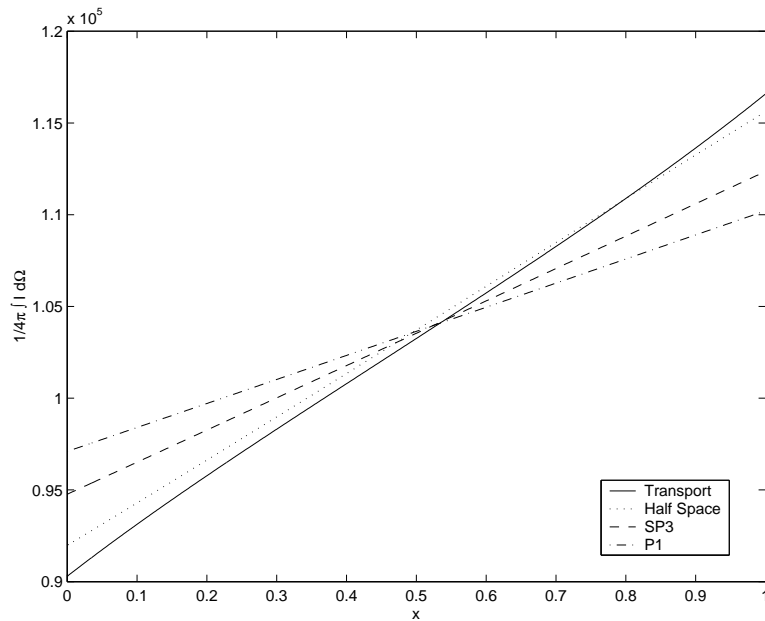


Figure 5.2: Incident radiation of the different models for a fixed temperature profile in 1D and  $\sigma = 0.1, \kappa = 0.01$ .

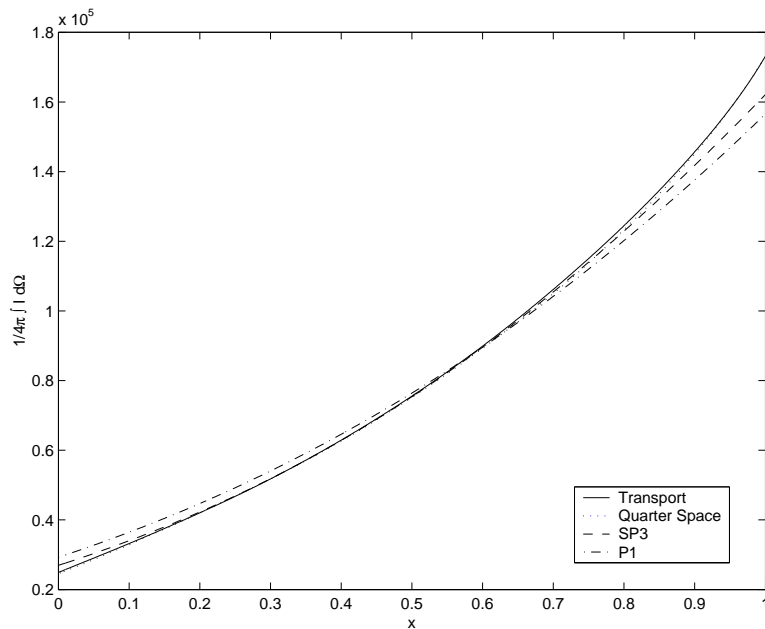


Figure 5.3: Incident radiation of the different models for a fixed temperature profile in 2D for  $\sigma = 1, \kappa = 1$ . Plot along the diagonal  $x = y$ .

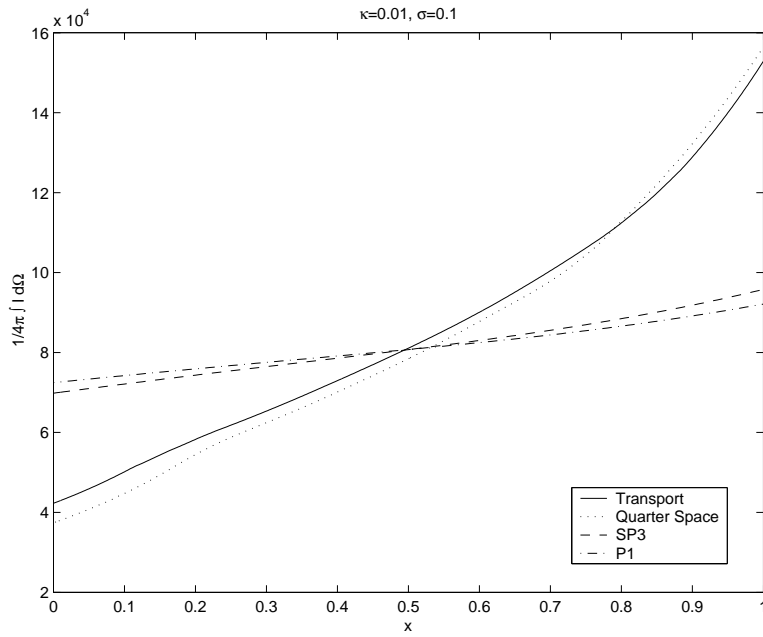


Figure 5.4: Incident radiation of the different models for a fixed temperature profile in 2D for  $\sigma = 0.1, \kappa = 0.01$ . Plot along the diagonal  $x = y$ .

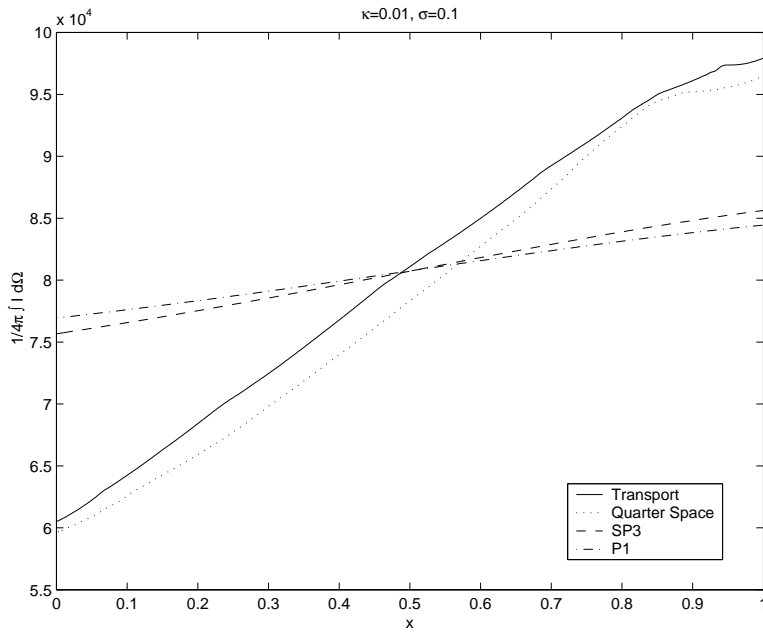


Figure 5.5: Incident radiation of the different models for a fixed temperature profile in 2D for  $\sigma = 0.1, \kappa = 0.01$ . Plot along  $y = 0.5$

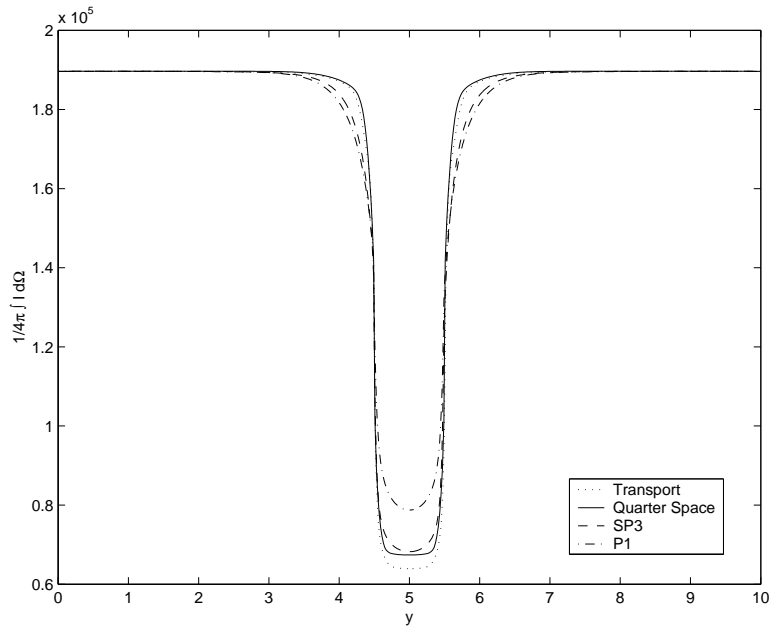


Figure 5.6: Incident radiation of the different models for discontinuous coefficients  $\kappa_0 = 3$ ,  $\kappa_1 = 1$ . Plot along  $x = 0.5$ .

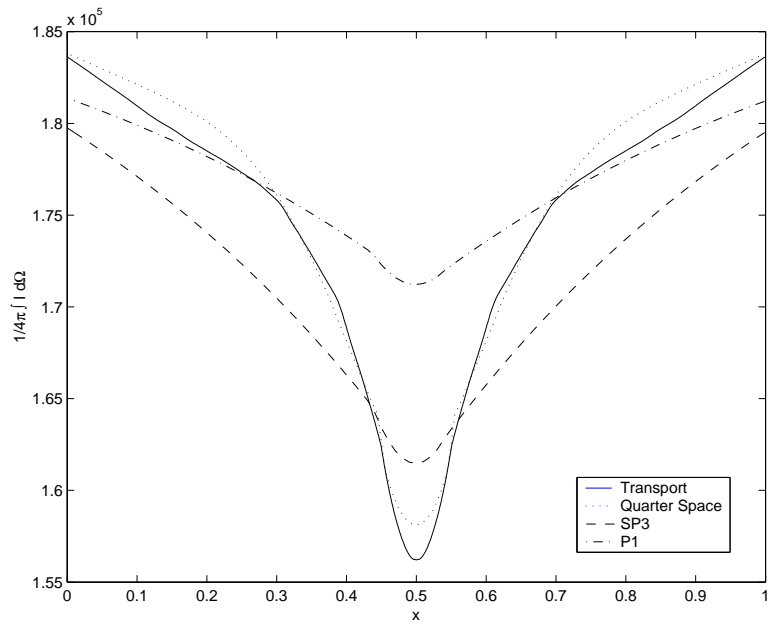


Figure 5.7: Incident radiation of the different models for discontinuous coefficients and  $\kappa_0 = 1$ ,  $\kappa_1 = 0.1$ . Plot along  $y = 5$ .

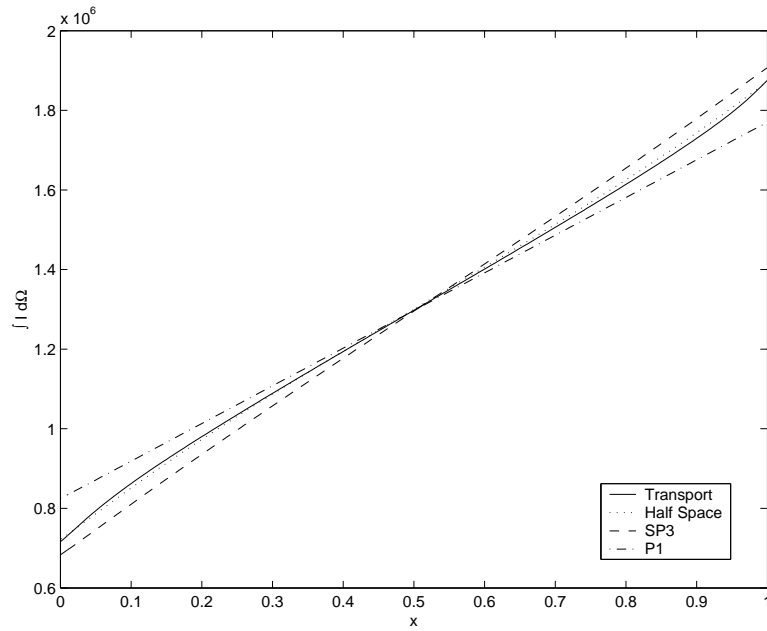


Figure 5.8: Incident radiation of the different models for the coupled equations in 1D with  $\kappa = 1$ .

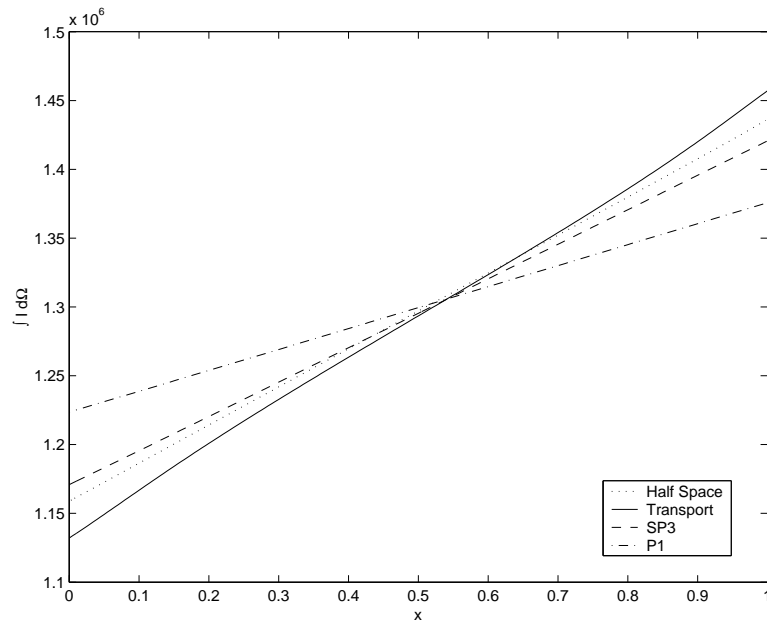


Figure 5.9: Incident radiation of the different models for the coupled equations in 1D with  $\kappa = 0.1$ .

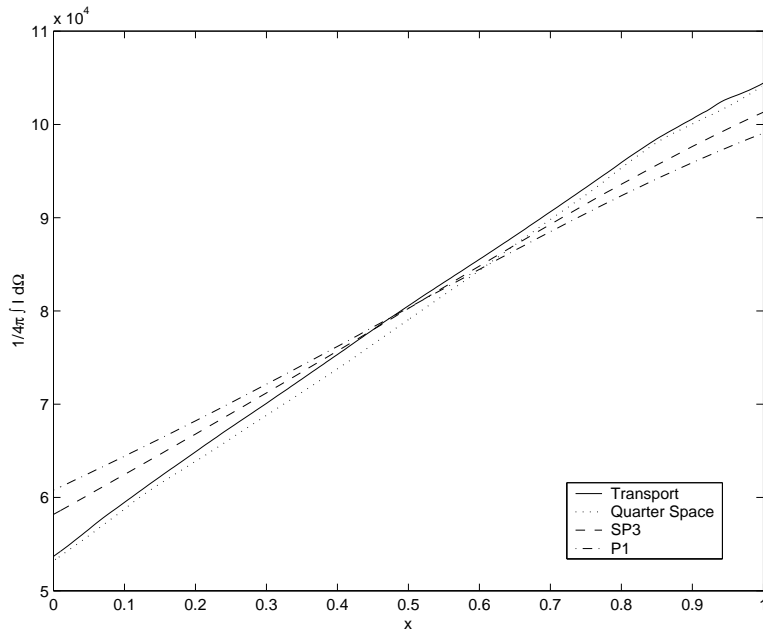


Figure 5.10: Incident radiation of the different models for the coupled equations in 2D for  $\kappa = 1$ . Plot along  $y = 0.5$ .

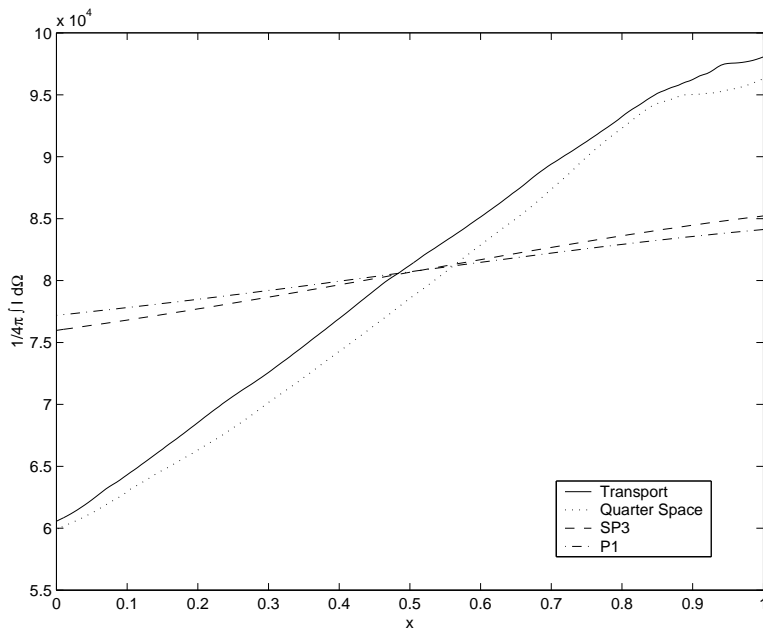


Figure 5.11: Incident radiation of the different models for the coupled equations in 2D for  $\kappa = 0.1$ . Plot along  $y = 0.5$ .

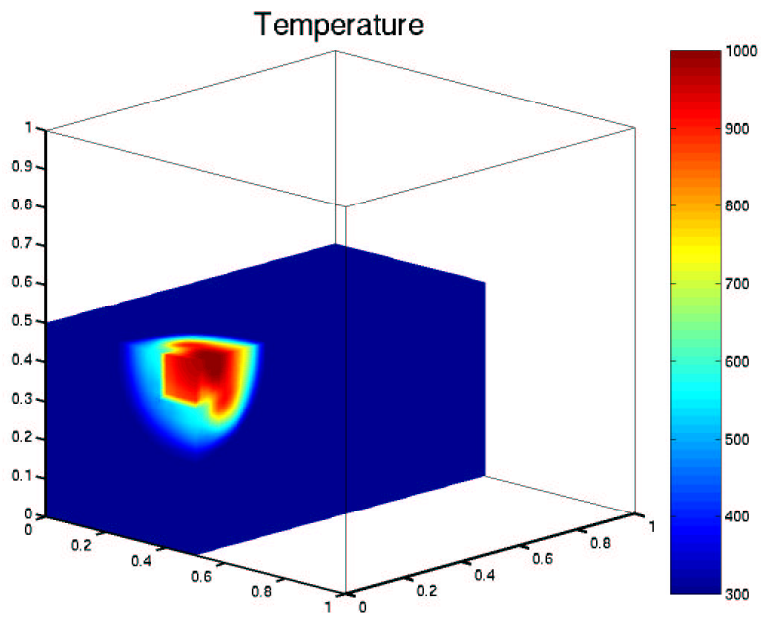


Figure 5.12: Temperature distribution for a flame-like flow

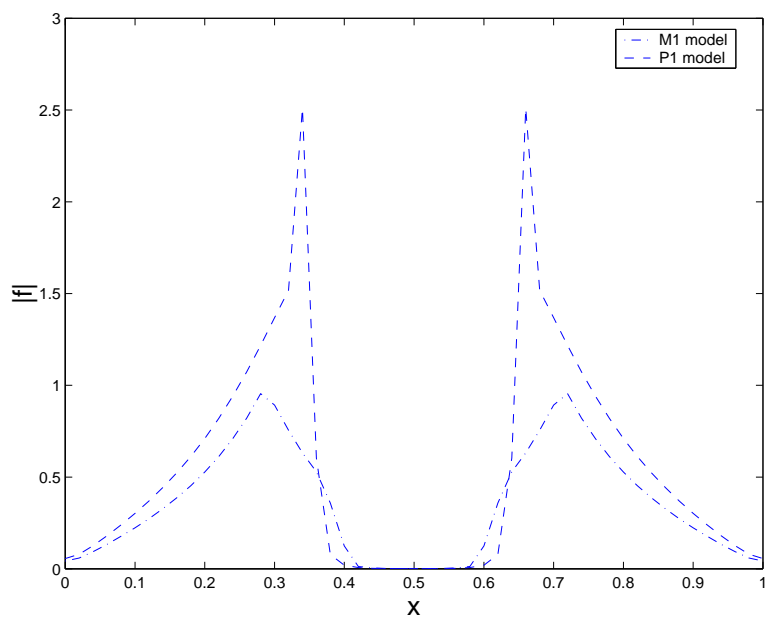


Figure 5.13: Norm of the relative flux